Journal of Medical Imaging

MedicalImaging.SPIEDigitalLibrary.org

Quantitative assessment of soft tissue deformation using digital speckle pattern interferometry: studies on phantom breast models

Udayakumar Karuppanan
Sujatha Narayanan Unni
Ganesan R. Angarai

SPIE.

Udayakumar Karuppanan, Sujatha Narayanan Unni, Ganesan R. Angarai, "Quantitative assessment of soft tissue deformation using digital speckle pattern interferometry: studies on phantom breast models," *J. Med. Imag.* **4**(1), 016001 (2017), doi: 10.1117/1.JMI.4.1.016001.

Quantitative assessment of soft tissue deformation using digital speckle pattern interferometry: studies on phantom breast models

Udayakumar Karuppanan,[a] Sujatha Narayanan Unni,[a,*] and Ganesan R. Angarai[b]
[a]Indian Institute of Technology Madras, Department of Applied Mechanics, Biophotonics Lab, Chennai, India
[b]Indian Institute of Technology Madras, Department of Physics, Applied Optics Lab, Chennai, India

Abstract. Assessment of mechanical properties of soft matter is a challenging task in a purely noninvasive and noncontact environment. As tissue mechanical properties play a vital role in determining tissue health status, such noninvasive methods offer great potential in framing large-scale medical screening strategies. The digital speckle pattern interferometry (DSPI)–based image capture and analysis system described here is capable of extracting the deformation information from a single acquired fringe pattern. Such a method of analysis would be required in the case of the highly dynamic nature of speckle patterns derived from soft tissues while applying mechanical compression. Soft phantoms mimicking breast tissue optical and mechanical properties were fabricated and tested in the DSPI out of plane configuration set up. Hilbert transform (HT)-based image analysis algorithm was developed to extract the phase and corresponding deformation of the sample from a single acquired fringe pattern. The experimental fringe contours were found to correlate with numerically simulated deformation patterns of the sample using Abaqus finite element analysis software. The extracted deformation from the experimental fringe pattern using the HT-based algorithm is compared with the deformation value obtained using numerical simulation under similar conditions of loading and the results are found to correlate with an average %error of 10. The proposed method is applied on breast phantoms fabricated with included subsurface anomaly mimicking cancerous tissue and the results are analyzed. [DOI: 10.1117/1.JMI.4.1.016001]

Keywords: breast phantom; digital speckle pattern interferometry; phase extraction; deformation; Hilbert transform; finite-element analysis.

Paper 16081PRRR received May 19, 2016; accepted for publication Jan. 6, 2017; published online Feb. 1, 2017.

1 Introduction

Research in the noninvasive assessment of tissues has been of increased interest in the recent past to consider the evolvement of patient-friendly diagnostic techniques at the clinical level. Even though mammogram, magnetic resonance imaging (MRI), and ultrasound techniques have emerged in a clinically usable level,[1] there are associated disadvantages in assessing malignancies related to specific tissue sites such as the breast. The major disadvantage is disease detection in one of its early developmental stages.[2] Fortunately, not all tissue lumps that are present within the breast will become a cancer, but there is a major possibility that unidentified long-term lesions/cysts may turn into a cancer.[3] Methods such as breast self-examinations (BSE) and clinical breast examinations (CBE) are used in breast screening for detecting suspicious masses or lesions by hand. For this, the lesion should be palpable and hence the size of the lesion creates a limitation here. The process also causes discomfort to the subjects due to physical contact.[4] Since the breast is a highly viscoelastic medium,[5] there is a great chance of missing the lesions in the above tests such as BSE and CBE. Identifying the cysts or lesions is the primitive step of diagnosing the tumor in early stages, which may not be always possible with the above methods. The current gold standard for breast cancer diagnosis is x-ray mammogram, ultrasonogram, positron emission tomography, and MRI. The pros and cons of these imaging modalities are well reported.[1,2,4] Recently, there have been reports investigating the potential of the mechanical properties of breast tissue such as elasticity, stiffness, and viscoelasticity as a discriminating factor in the course of a developing malignancy, which can be quantified to classify the pathological changes.[6] Common types of breast cancers are of epithelial origin.[7] The accumulation of cells or formation of cysts/lesions has a positive growth rate toward the inner layers in the case of breast sarcomas.[8] Due to the changes in cell metabolism that occur during the development of cancer, the above-mentioned mechanical properties will undergo changes and the quantification and comparison of these properties with that of the normal control site can result in the evaluation of the tissue status. Some of the *in vivo* techniques approved clinically to characterize the tissue stiffness and elasticity properties are ultrasound elastography and MRI.[9–12] Looking at the difference in the deformation profile of normal and malignant tissues would be of additional advantage in characterizing malignancies.[13] We had previously demonstrated an optical method based on DSPI configuration to classify the normal and abnormal breast phantoms on a qualitative scale,[14] by just noticing the fringe deviations at the location of the abnormality. An attempt to quantify the deformation of the breast tissue is carried out in this paper. The normally

*Address all correspondence to: Sujatha Narayanan Unni, E-mail: nsujatha@iitm.ac.in

2329-4302/2017/$25.00 © 2017 SPIE

practiced temporal phase shifting method for phase and subsequent deformation extraction from the obtained fringes would not be realistic here due to the highly decorrelating nature of speckle patterns obtained from soft tissues.[15] Hence, we have demonstrated a Hilbert transform (HT)-based phase extraction algorithm from a single fringe image experimentally acquired from the sample. The algorithm is validated using simulated fringes from a standard circular diaphragm with arrested edges and the results are found to be satisfactory. The applicability of the algorithm on the fringes obtained from a breast phantom is again verified with numerically simulated deformation profiles using Abaqus finite-element analysis algorithm. The experiments are extended with a nonhomogeneous phantom representing malignancy and the extracted deformation is found to be clearly different from that of its homogeneous counterpart.

2 Materials and Methodology

2.1 *DSPI Theoretical Background for Cone-Shaped Model*

The fringe formation in DSPI based on the intensity correlation of the speckle patterns before and after object loading is well reported.[16] In the equations given below, I_0 and I_R are the intensities of the object beam and reference beam, respectively. The resultant intensity in the image plane before applying displacement is given by

$$I = I_o + I_R + 2\sqrt{I_o I_R}\ \cos\ \varnothing, \tag{1}$$

where $\varnothing$ is the phase difference between the two beams.

The resultant intensity of the image after object displacement is given by

$$I = I_o + I_R + 2\sqrt{I_o I_R}\ \cos(\varnothing + \delta), \tag{2}$$

where δ is the additional phase change introduced due to the specimen displacement.

This additional phase change could be expressed and extracted in terms of the illumination geometry as well as the applied compression vectors considering a three-dimensional (3-D) geometry.[17] However, depending on the shape of the interrogated 3-D geometry, the obtained phase change reflecting the amount of deformation undergone by the specimen will vary and hence the fringe formation equations in the present case are detailed here. The displacement vector was derived in cylindrical co-ordinates. In this derivation, the illumination and imaging vectors are oriented toward the outer curved surface of a truncated cone geometry representing the breast phantom. Depending on the type of loading, the magnitudes of net displacement vector **D** of any point in the specimen when represented in cylindrical co-ordinates can be resolved along the r (radial), t (tangential—an approximation for θ for small deformations), and a (axial) directions, are denoted as D_r, D_t, and D_a, respectively, and are shown in Fig. 1. Therefore, the small deformation vector of the specimen at point P upon compression loading along the axial direction is given by

$$\mathbf{D} = D_a\mathbf{i}_a + D_r\mathbf{i}_r + D_t\mathbf{i}_t, \tag{3}$$

where $\mathbf{i}_r$, $\mathbf{i}_a$, and $\mathbf{i}_t$ represent the unit vectors in the radial, axial, and tangential directions.

Here, the magnitude and direction of net deformation components depend on the amount of deformation of the specimen location along the specified axes which in turn depends on the cone angle and the specific loading conditions. Figure 1 shows the vector diagram of the light intensity for a cone model in an out of plane DSPI set-up.

Let $\mathbf{k}_1$ and $\mathbf{k}_2$ be the unitary vectors indicating the directions of illumination and observation

$$\mathbf{k}_1 = -\mathbf{i}_a\ \sin\ \theta_i - \mathbf{i}_r\ \cos\ \theta_i, \tag{4}$$

$$\mathbf{k}_2 = \mathbf{i}_r, \tag{5}$$

$$\delta = \left(\frac{2\pi}{\lambda}\right)(\mathbf{k}_2 - \mathbf{k}_1)\cdot\mathbf{D}, \tag{6}$$

where λ is the wavelength of the illumination light. The phase change due to specimen deformation is given by

$$\delta = \frac{2\pi}{\lambda}(\mathbf{i}_r + \mathbf{i}_a\ \sin\ \theta_i + \mathbf{i}_r\ \cos\ \theta_i)\cdot\mathbf{D}, \tag{7}$$

$$\delta = \frac{2\pi}{\lambda}(\mathbf{i}_r + \mathbf{i}_a\ \sin\ \theta_i + \mathbf{i}_r\ \cos\ \theta_i)\cdot(D_r\mathbf{i}_r + D_a\mathbf{i}_a + D_t\mathbf{i}_t), \tag{8}$$

$$\delta = \frac{2\pi}{\lambda}[\sin\ \theta_i D_a + (1 + \cos\ \theta_i)D_r]. \tag{9}$$

From Eq. (9), it is clear that the D_r component (out of plane) has more sensitivity in forming the fringe pattern. However, the axial component of deformation also has sensitivity in the fringe

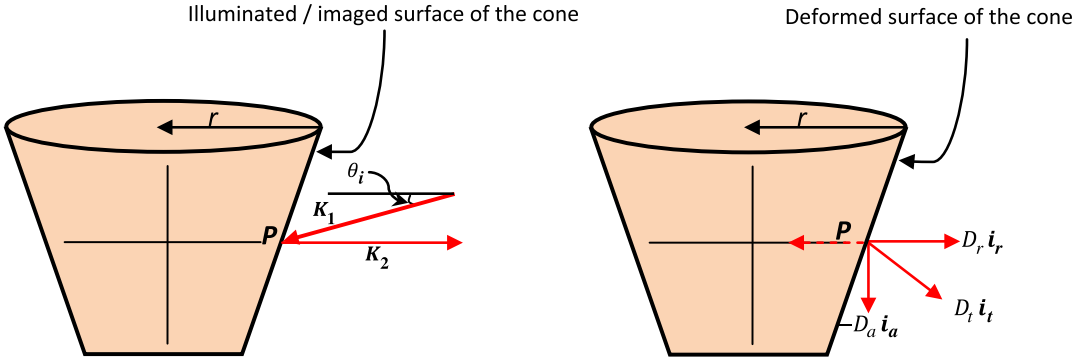

Fig. 1 Vector diagram of light intensity for a cone model in the out of plane DSPI configuration. (a) Illumination and imaging vectors and (b) deformation vector components.

pattern, which arises due to the shape of the sample. In the current experimental set up, Eq. (9) is used for calculating the phase change introduced on the curved surface due to the deformation upon the application of a compression load along the axis of the cone. The effect of this phase change in modulating the brightness/darkness of the interference pattern representing the fringes is well reported in the literature.

2.2 *Experimental Set-Up*

Figure 2 shows the schematic diagram of the out of plane DSPI set-up for testing the sample specimens. The output beam from a 632.8-nm helium neon laser (source) is divided in two using a beam splitter-1 (BS-1). The spatially filtered divergent transmitted beam is used to illuminate the sample with the help of mirror M4. The diffused back scattered light from the sample is allowed to combine with the reference beam with the help of a second-beam splitter/combiner (BS-2). Mirrors M2, M3, and the ground glass (reference) combination were arranged according to Fig. 2 to facilitate the steering of the reference beam. A charge coupled device (CCD) camera—zoom lens combination (Sony XC-ST 70CE—optem macro lens)—was used to capture the combined image from the sample and reference surfaces. The CCD is connected to a frame grabber interfaced with a computer. Using the developed algorithm, the phantom image was captured and served as the reference image. The sample was uniformly compressed at predefined values at the minimum diameter area using a digital micrometer head loading system (Mitutoyo). The deformed image of the sample is captured in real time and subtracted from the stored reference image using the developed algorithm at a rate of 25 frames/s to visualize the deformation fringes.[18]

2.3 *Preparation of the Breast Phantom*

Phantoms were prepared to mimic the optical and mechanical properties of the normal/abnormal breasts. The ingredients used for making these phantoms were regular grade agar powder (SRL Chemicals, India) which mimics the stiffness of the real breast tissue, Intralipid 20% (Fresenius Kabi, Germany) which mimics the breast scattering properties, and dye-based black India ink (Bril, India) for mimicking absorption of the abnormal tissue.[19] The use of increased agar concentration increased the stiffness of the phantom which mimicked the abnormal tissue.[20] For the fabrication of the normal phantom, 4 g of agar powder is dissolved in 200 ml of distilled water. This solution is stirred continuously while heating to 75°C. At this point, the solution is allowed to cool down to 60°C following which 4.5 ml of 20% Intralipid is added to the solution. The mixed solution is poured into a conical mold and allowed to cool to room temperature. The prepared phantom (hereafter referred to as sample 1) is shown in Fig. 3(a). In order to mimic a tumor region with increased stiffness, 8 g of agar is used as the base with an added 10 μl of India ink. The India ink is added to mimic the increased absorption of a malignancy. A tumor of size 1 cm with a thickness 0.5 mm was cut from this phantom and incorporated as an anomaly representing flat dysplasia into the normal phantom. The prepared inclusion was placed ~1 mm from the outer surface of the phantom as shown in Fig. 3(b). Figure 3(c) shows the anomaly included phantom (hereafter referred to as sample 2). After placing the inclusion, the remaining volume of the mold was filled with the normal phantom mixture without disturbing the position of the inclusion.

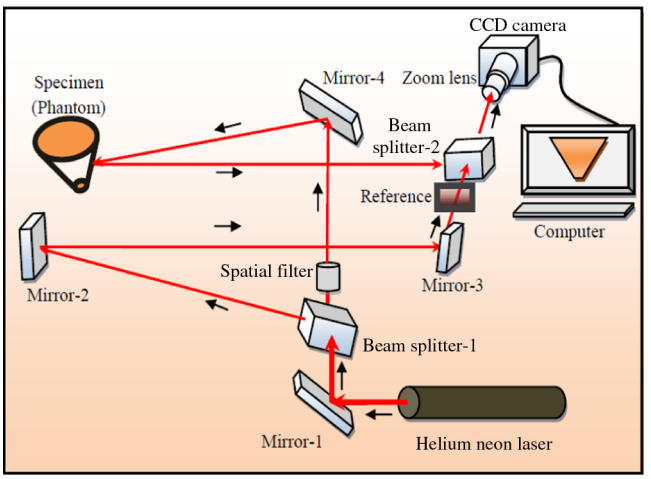

Fig. 2 Schematic of the out of plane DSPI configuration.

2.4 *Breast Phantom Mechanical Characterization Using Ultrasound*

The material properties of the normal breast phantom and the inclusion were characterized using the ultrasound probe (Olympus, 1 MHz) test as shown in Figs. 4(a) and 4(b). The ultrasound testing was carried out by placing the transducer directly over the phantom surface. The sample was tested for both longitudinal and transverse waves of sound propagation at multiple points with a constant height (h) as shown in Fig. 4(a). First, the sample was wiped with tissue paper to remove the extra water content over the area to be tested. To have proper conduction of sound, an ultrasound gel was applied over the surface of the sample and the probe was placed over it. By measuring the time of flight and knowing the sample height, the elastic constants of the material were estimated. Estimated speed of sound in the breast phantom closely matched that of the real breast tissue[20] (1430 m/s for normal phantom and 1420 m/s for inclusion). The Young's modulus and Poisson's ratio of the normal phantom were estimated to be 15.9 kPa and 0.46, whereas the abnormal inclusion gave the values of 33.78 kPa and 0.5. All these values correlated well with the existing literature on the elastic properties of breast tissues.

As mentioned in Sec. 1, the DSPI technique has an inherent advantage in characterizing the tissue deformation in a whole field, noncontact, and real-time environment and has the potential of offering quantitative information about the deformation. In addition, it is useful for identifying tissue abnormalities in subsurface layers.[21] However, the effective extraction of information from the obtained fringes purely depends on the adapted image analysis methods. The proposed image analysis associated with DSPI offers less computational time and low-memory consumption at low cost. There are well-established techniques to extract the phase and quantify the deformation from DSPI fringe pattern images,[22] however, only for rigid engineering samples. One of the best ways to extract the deformation is by using a temporal phase shifting technique involving piezo electric transducers to change the path length of the beam. The limitations in implementing the temporal phase shifting for biological soft tissue are its viscoelastic nature causing fast stress distribution and subsequent decorrelation of speckle

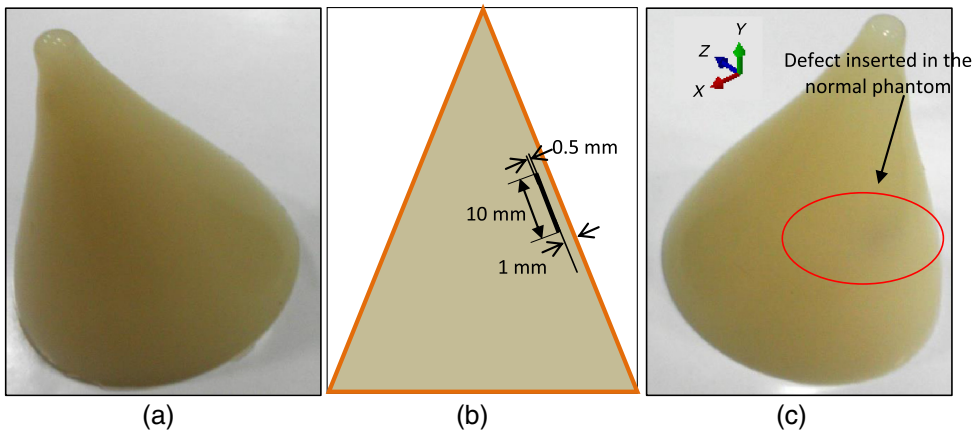

Fig. 3 (a) Agar gel cone normal phantom, (b) defect inclusion, and (c) abnormal phantom.

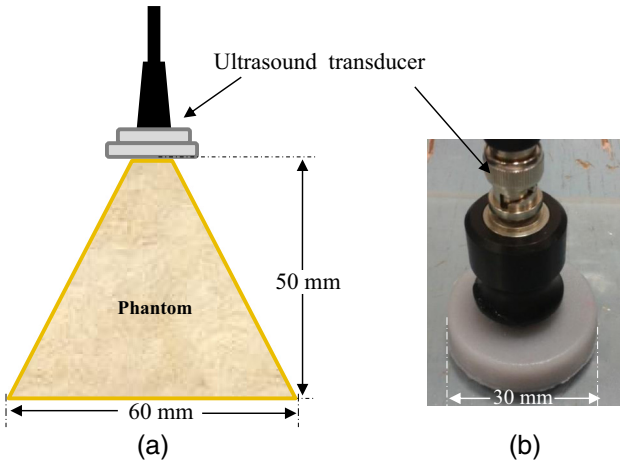

Fig. 4 Ultrasound testing of (a) cone phantom and (b) anomaly.

patterns. Extraction of phase from a single interferogram would be a better option to be used in such scenarios and the principle and the methods adopted for the same are described below.[23]

2.5 *Processing of DSPI Images*

The processing of DSPI images to extract the hidden phase as well as deformation information is a challenging task especially in the case of soft samples such as tissue. The various processes involved the extraction methodology are given below.

2.5.1 *Image contrast enhancement*

The fringe pattern obtained for the normal breast phantom using the experimental system described previously is shown in Fig. 6(a). An extracted deformation profile relies on retrieving the optical phase information from the interferometric fringe patterns and the subsequent method of phase unwrapping. To start the process, noisy speckle images were filtered using a median filter as reported in the literature.[24] The fringe pattern contrast and visibility were enhanced by using a median filter of window size 3×3 applied to the image. Choice of the smaller window size improved the filtering results and also maintained the low-frequency information in the image.

2.5.2 *Phase extraction*

Phase extraction from a single interferogram is really challenging and has been reported earlier in engineering specimens. Some of the practices developed earlier for this purpose include usage of windowed Fourier transform, Goldstein's branch cut algorithm, quality-guided path following method, weighted least-square method, and minimum Lp-norm phase unwrapping method. The main sources of error in obtaining the phase from a single interferogram is due to unavoidable noise, data inconsistency, and loss of data and invalid area particularly due to shape of the sample.[25] Most of above-mentioned phase unwrapping methods could not deal with the above-mentioned errors, especially the noise and abrupt phase change. Another reported method called the extreme map method worked better, but was applicable only for closed loop fringes. In this case, the deformation of the breast phantom resulted in open loop curved fringes with alternate dark and bright intensity distributions over the image pixels. After careful review of the various image processing methods mentioned above, we have adopted he HT-based method for extracting the wrapped phase distribution from the soft breast phantom fringes.[26] As explained in Sec. 2, the phase of the image contains the information about the object's deformation. The image is transformed to a complex plane by applying HT. The wrapped phase image is obtained using the following equation:

$$W = a \tan\left[\frac{H_i(I)}{I}\right], \tag{10}$$

where $H_i(I)$ is the imaginary part of the original image (I) after applying the HT and W is the wrapped phase image. The hidden phase values from the wrapped phase image ranging from $-\pi$ to $+\pi$ are unwrapped using the multigrid method to get the continuous phase map. The obtained phase map is further filtered and smoothed using discrete cosine transform.[27]

2.6 *Finite Element Method Analyses on Breast Phantom Model*

Finite-element method analysis of the breast phantom model was carried out using Abaqus 6.10, in order to understand the stress distribution in the sample while applying a specific external load. For simulation, a 3-D truncated cone matching real phantom dimensions was modeled using Abaqus part

module. The mechanical properties such as elastic modulus and Poisson's ratio of the breast phantom were estimated by the ultrasound method as discussed in Sec. 2.4. These estimated mechanical properties were assigned to the model using a material property module. The cone was modeled without anomaly inclusion considered analogous to homogeneous normal phantom and its deformation analysis was carried out to visualize the stress distribution over its outer surface. The model was meshed using quadratic tetrahedron element with an element size of 45,530. The selection of this element size was based on an optimization between the accuracy of the obtained results and the computational time. All degrees of freedom on the large diameter of the cone were arrested using the encastre boundary condition. The smaller diameter of the cone bottom was subjected to a uniform body force along the y-axis and its deformation contour was plotted. This procedure was repeated for multiple applied values of deformation.

3 Results

3.1 *Validation of the Developed Algorithm*

The developed algorithm for the phase extraction from a single fringe image was validated by applying it to a computer simulated circular fringe of a centrally loaded circular diaphragm with its edges arrested as shown in Fig. 5(a). Figure 5(b) shows the unwrapped phase plot obtained using the developed algorithm and Fig. 5(c) shows the two-dimensional (2-D) deformation distribution plot in a false color mapped version, whereas Fig. 5(d) shows it in 3-D. The deformation plot was obtained by multiplying the extracted phase distribution plot [Fig. 5(b)] with $\frac{\lambda}{4\pi}$, at all pixel coordinates, ($\lambda = 632.8$ nm), according to the small angle of illumination approximation as explained in Sec. 2.1.[28] The deformation values are found to correlate with the applied deformation (0.5 μm) at the center of the diaphragm.

3.2 *Comparison of Experimental Fringes with Numerical Simulation Results*

The experimental fringe patterns obtained for sample 1 under different conditions of applied deformation is shown in Figs. 6(a) to 6(c). Figures 6(a) to 6(c) show the fringes obtained for 4, 5, and 6 μm applied deformations.

The number of fringes increased with an increase in applied deformation indicating the increased deformation over the sample volume as expected. For numerical simulations, the conditions of loading were mimicked by selecting the body force model as for a soft gel sample, with the applied deformation spread over the entire volume of the body. Body force values of 4, 5, and 6 N/m^3 were selected to represent the maximum vertical displacement at the sample area in contact with the applied deformation unit in line with that of the experiments (4, 5, and 6 μm).

It was observed that for increased values of applied deformation, the fringe pattern appeared random and dynamic for the hydrogel-based soft phantom. The dynamic nature of the phantom made fringes disappear suddenly because of the increased applied stress. Since the sample was a gel (due to its viscoelastic property, the fringes decorrelated (disappeared) when subjected to deformations greater than 12 μm. It was observed that for the selected range of deformation (4 to 6 μm), the stress distribution in the sample was uniform as evident from the obtained uniform fringe patterns.

3.3 *Image Analysis for DSPI Fringes from Normal and Abnormal Breast Phantoms*

After the validation explained in Sec. 3.1, the algorithm was applied to sample 1 and the results are shown in Fig. 7. DSPI fringe obtained for sample 1 is shown in Fig. 7(a). Figure 7(b) shows unwrapped phase plot obtained using the developed algorithm and Fig. 7(c) shows 2-D deformation distribution plot in a false color mapped version, whereas Fig. 7(d) shows the 3-D surface deformation profile.

DSPI fringe obtained for sample 2 is shown in Fig. 8(a). Figure 8(b) shows the unwrapped phase plot obtained using the developed algorithm and Fig. 8(c) shows the 2-D deformation distribution plot in a false color mapped version, whereas Fig. 8(d) shows the 3-D surface deformation profile.

3.4 *Comparison of Anomaly Location*

The spatial location of the anomaly was identified by comparing the images in Fig. 9. In sample 2, subsurface anomaly $(10 \times 10 \times 0.5)$ mm^3 was embedded at a height of 18 mm from the X-axis and 30 mm from the Y-axis. This anomaly location was experimentally detected using DSPI technique by observing the fringes and extracting the hidden optical phase and unwrapping it from the speckle deformation fringe pattern. The stress accumulation due to anomaly inclusion was evident in the formed fringe pattern [Fig. 9(b) represented by the deviation in fringes] and deformation profile [Fig. 9(c) represented by the decrement in deformation value] at the same location of the anomaly as that of the original phantom. Thus, the

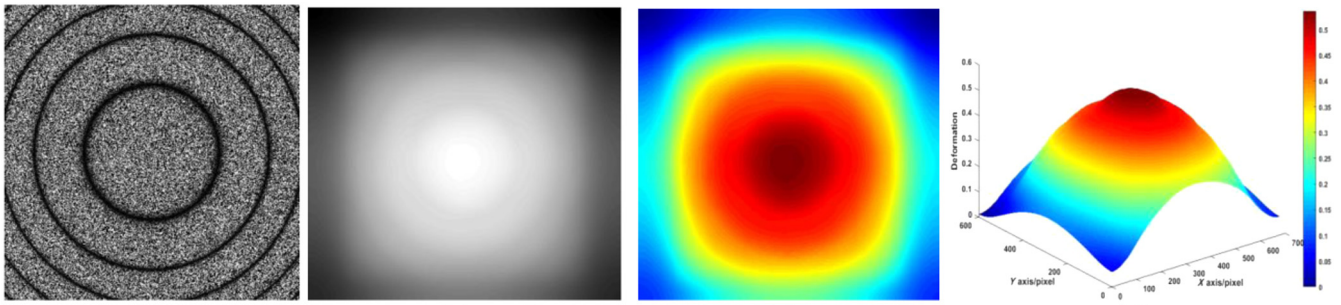

Fig. 5 Extraction of deformation from a single interferogram (simulated fringe pattern from centrally loaded circular diaphragm). (a) Original image, (b) unwrapped phase map, (c) false color representation of surface deformation distribution (c) in 2-D (d) in 3-D.

Applied deformation	4 μm	5 μm	6 μm
DSPI fringe pattern	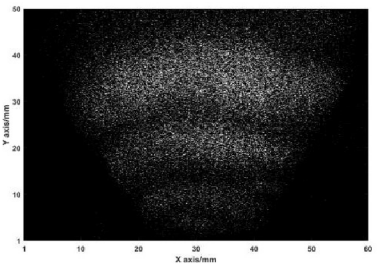	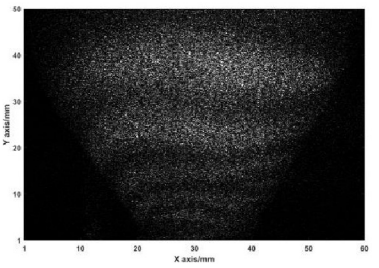	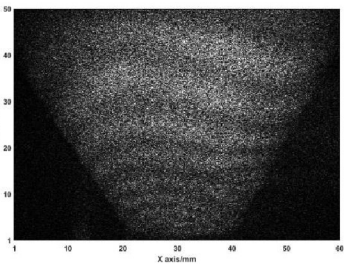
	(a)	(b)	(c)
Simulated fringe contour	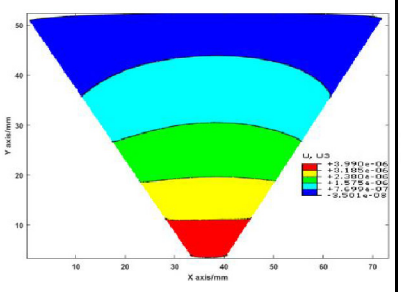	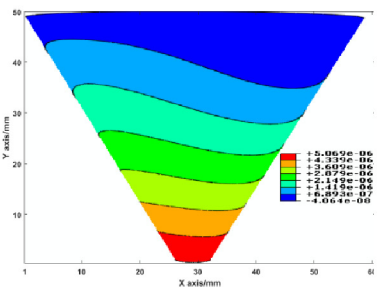	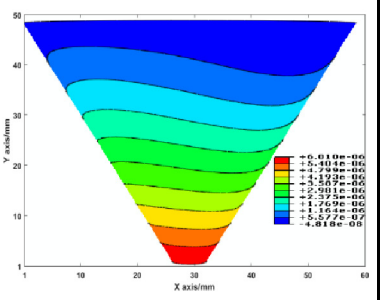
	(d)	(e)	(f)
Deformation profile (2-D)	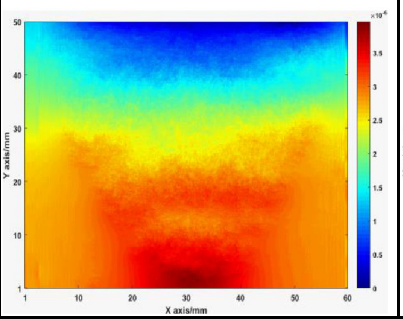	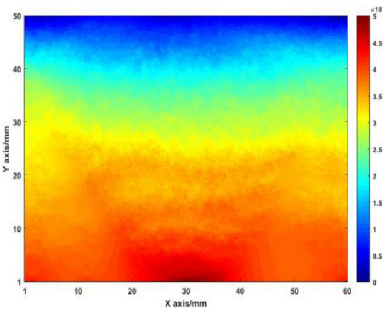	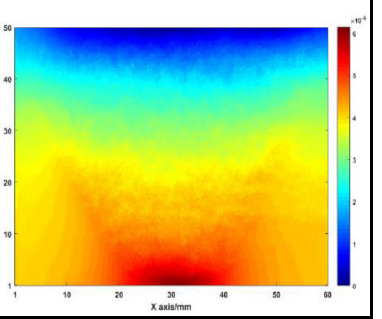
	(g)	(h)	(i)

Fig. 6 Comparison of experimental fringe patterns (a)–(c) and numerically simulated results (d)–(f) and 2-D deformation profile for sample 1 under different applied deformations.

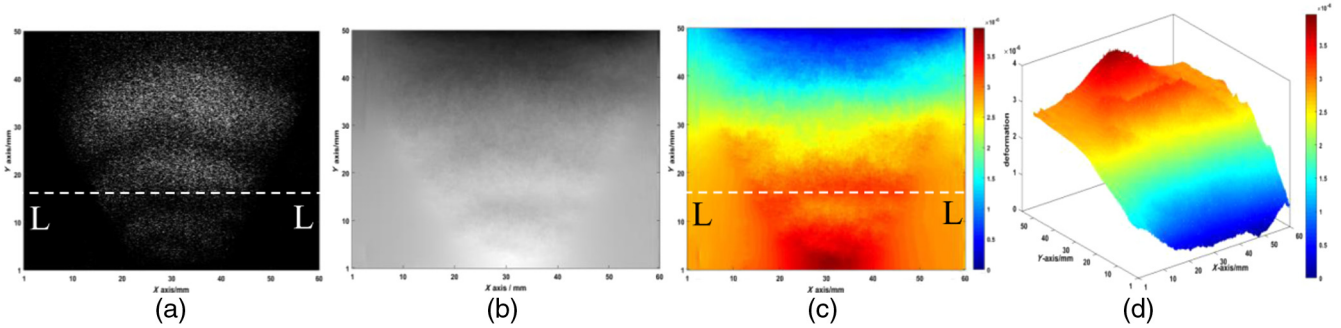

Fig. 7 Deformation extraction from a single interferogram for an applied deformation of 4 μm to sample 1. (a) Original image, (b) unwrapped phase map, (c) 2-D deformation distribution false color map, and (d) 3-D surface deformation distribution.

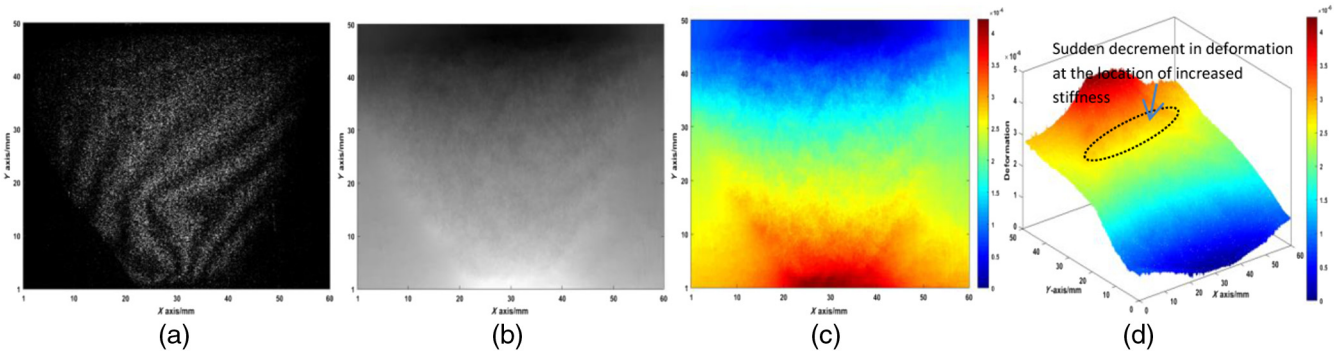

Fig. 8 Deformation extraction from a single interferogram for an applied deformation of 4 μm to sample 2. (a) Original image, (b) unwrapped phase map, (c) 2-D deformation distribution false color map, and (d) 3-D surface deformation distribution.

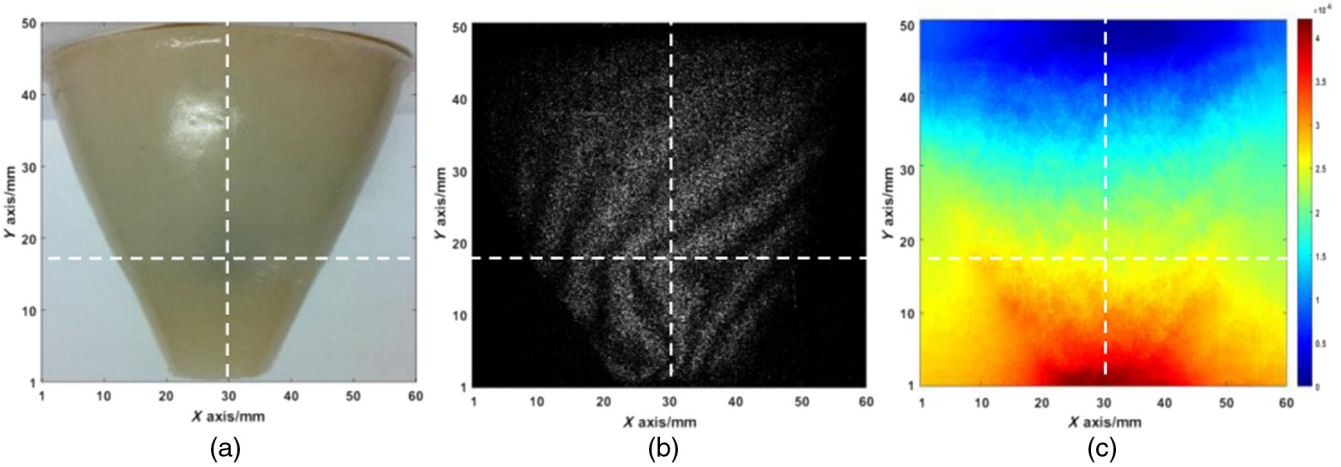

Fig. 9 Sample 2: (a) photograph, (b) experimental fringe pattern for an applied deformation of 4 μm, and (c) 2-D deformation profile for the applied deformation. A horizontal line drawn at 18 mm from *x*-axis and a vertical line drawn at 30 mm from *y*-axis intersects shows the abnormal location.

anomaly location was estimated quantitatively based on the distance approach.

4 Discussions

4.1 *Applicability of the Algorithm in Single Fringe Pattern-Based Deformation Extraction*

The developed algorithm was validated using a simulated fringe pattern for a centrally loaded circular diaphragm with arrested edges as shown in Figs. 5(a)–5(d). The unwrapped phase obtained using the HT-based algorithm [Fig. 5(b)] showed uniform variation with the maximum value of phase change at the center and zero value of deformation at the arrested edges. Extracted deformation, Fig. 5(d), also followed the same trend and was found to follow the reported literature,[28] thus validating our algorithm.

As represented in Fig. 6, the numerically simulated deformation contours [Fig. 6(d)] were found to follow the same trend as the experimental fringes [Fig. 6(a)], for a specific applied deformation of 4 μm, verifying the nature of spread of the applied deformation in a soft gel phantom. The trend was observed to be similar for different values of applied deformation [Figs. 6(e) and 6(b) for 5 μm and Figs. 6(f) and 6(c) for 6 μm].

4.2 *Numerical Comparison of the Extracted Deformation Profile*

The deformation values at different spatial locations of the sample obtained using simulations were compared with the extracted 2-D deformation profile from the experimentally acquired fringes. Figure 7 shows the deformation extraction sequence using the developed algorithm for a 4 μm applied deformation for sample 1. In both simulations [Fig. 6(d)] and the extracted deformation profile [Fig. 7(c)], the variation of deformation was observed to be uniformly spread out from a maximum (at the applied deformation point) to a minimum (at the supported base). A close correlation was observed between the extracted deformation values as well as the originally applied deformation values under various applied deformation conditions. The errors associated with maximum and minimum values of deformation for experimentally extracted and simulated profiles are found to be within 2% variation for different applied values of deformation. For comparing the experimentally extracted and simulated values, multiple points along the same vertical height in the sample in each of the major color bands of the sample deformation profile were considered. The average %error in comparing the extracted and simulated values for different color bands was found to be

within the limit of 10%. These comparisons confirmed the applicability and validity of extracting deformations using the proposed methodology.

4.3 *Extension of Experiments with Nonhomogeneous Phantom (Sample 2)*

To extend the application of the proposed DSPI-based deformation analysis on soft tissue phantoms, experiments were carried out with sample 2 and the corresponding results obtained are shown in Fig. 8. While the maximum and minimum values for sample 2 deformation were found to correlate with that of sample 1, the deformation values at the location of abnormality showed a sudden decrement in sample 2 [Fig. 8(d)] as compared to the corresponding location in sample 1 [Fig. 7(d)]. However, it is worth noting that the phase as well as the deformation distribution has some residual noise at random locations, which is clear in a 3-D plot and this could be purely attributed to the efficiency of the filtering process. Filtering the DSPI fringe images, especially for a soft tissue phantom, is a challenging task and has to be specifically designed considering the sample in question. However, in a 2-D representation, this effect could be minimized and hence we have used a 2-D deformation distribution plot for further comparisons. Localized deformation values along a line L-L drawn at the same vertical height in the extracted 2-D deformation profiles were considered for the comparison. The decrement in deformation at the position of increased stiffness was evident along L-L in Fig. 8(c) as compared to Fig. 7(c). Also, it was noted that the change in sample deformation at the position of abnormality was much larger (>10 times) than the estimated errors as explained in Sec. 4.2, proving that the predominant reduction in the deformation was necessarily due to the presence of an abnormality.

The presence of the abnormality was also clearly evident from the obtained fringe pattern in Fig. 8(a). As compared to its normal counterpart (sample 1), the fringes were clearly deviated from a normal profile [Fig. 7(a)] for the same applied load. Further processing of the fringe pattern also provided us with the amount of reduction in the sample deformation as a result of the accumulated stress in the region of abnormality, representing a tissue mass of high stiffness. Precise localized tumor margin assessment requires further processing and experimentation which will be dealt with in future.

5 Conclusions

The quantitative assessment of soft tissue deformation using DSPI is demonstrated in this paper. The experiments were carried out in breast mimicking phantoms having the optical and mechanical properties of real breast tissue. In general, the DSPI fringes obtained from soft tissue phantoms/organs are highly decorrelating in nature with the applied load. Hence, a single interferogram-based method is developed here for optical phase extraction as well as deformation assessment with the help of the HT-based technique on open loop fringe patterns. The quantification of out-of-plane deformation of breast phantom is accomplished using this proposed method.

Mapping the deformation profile of a highly viscoelastic medium such as breast for an applied load/force is a challenging task and this paper shows the applicability of the same using DSPI-based methods with the least computational cost. Furthermore, the entire DSPI could be miniaturized, which gives an additional advantage for *in vivo* applications. The applied load range mentioned in this study could be realized by appropriate thermal loading when used under clinical testing conditions. The close correlation of numerical and developed tissue phantom deformation information could further be expanded using optimization strategies to extend this concept to the estimation of mechanical properties of soft tissues, which are found to vary during disease progression. As noncontact and very minimal invasive techniques, DSPI-based methods could thus extend the possibilities in extracting soft tissue mechanical properties, which offers potential applications in developing real-time diagnostic optical tools in cancer research.

Disclosures

No conflicts of interest, financial or otherwise, are declared by the authors.

Acknowledgments

The authors acknowledge Centre for Non Destructive Evaluation, IIT Madras for providing facility for the ultrasound testing of the tissue phantom model.

References

1. J. M. Park and D. M. Ikeda, "Promising techniques for breast cancer detection, diagnosis, and staging using non-ionizing radiation imaging techniques," *Phys. Med.* **XXI**(I) (2006).
2. J. A. Smith and E. Andrepoulou, "An overview of the status of imaging technology for breast cancer," *Ann. Oncol.* **15**(Suppl. 1), I18–I26 (2004).
3. O. Warburg, "On the origin of the cancer cells," *Science* **123**(3191), 309–314 (1956)
4. A. B Nover et al., "Modern breast cancer detection: a technological review," *Int. J. Biomed. Imag.* **2009**, 1–14 (2009).
5. S. Suresh, "Biomechanics and biophysics of cancer cells," *Acta Mater.* **55**, 3989–4014 (2007).
6. M. R. Vegas and J. L. Matrin del Yerro, "Stiffness, compliance, resilience, and creep deformation: understanding implant-soft tissue dynamics in the augmented breast: fundamentals based on materials science," *Aesthetic Plast. Surg.* **37**(5), 922–930 (2013).
7. E. T. Crook, E. W. Thompson, and J. P. Thiery, "Epithelial to mesenchymal transition and breast cancer," *Breast Cancer Res.* **11**, 213 (2009).
8. T. D. Pencavel and A. Hayes, "Breast sarcoma—a review of diagnosis and management," *Int. J. Surg.* **7**, 20–23 (2009).
9. T. A. Krouskop et al., "Elastic moduli of breast and prostate tissues under compression," *Ultrason. Imaging* **20**(4), 260–274 (1998).
10. S. J. Kirkpatrick, "Optical assessment of tissue mechanical properties," *Proc. SPIE* **4001**, 92–101 (2000).
11. R. Sinkus et al., "Imaging anisotropic and viscous properties of breast tissue by magnetic resonance-elastography," *Magn. Reson. Med.* **53**, 372–387 (2005).
12. C. V. Santiago-Lona et al., "Non-destructive optical methods for the study of soft tissues," *Proc. SPIE* **9660**, 966012 (2015).
13. H. Hong, D. B. Sheffer, and C. W. Loughry, "Detection of breast lesions by holographic interferometery," *J. Biomed. Opt.* **4**(3), 368–375 (1999).
14. K. Udayakumar, N. Sujatha, and A. R. Ganesan, "Digital speckle pattern interferometry based anomaly detection in breast mimicking phantoms: a pilot study," *Proc. SPIE* **9417**, z1–z7 (2015).
15. K. Creath, "Phase-shifting speckle interferometry," *Appl. Opt.* **24**(18), 3053–3058 (1985).
16. U. P. Kumar, N. K. Mohan, and M. P. Kothiyal, "Interferogram analysis using Hilbert transform," in *Int. Conf. on Optics and Photonics, Proc. ICOP*, Optical Interferometry, Holography & Laser Speckles, Chandigarh, India (2009).
17. N. U. Sujatha and V. M. Murukeshan., "Nondestructive inspection of tissue/tissue like phantom curved surfaces using digital speckle shearography," *Opt. Eng.* **43**(12), 3055–3060 (2004).
18. S. Schedin, G. Pedrini, and H. J. Tiziani, "Pulsed digital holography for deformation measurements on biological tissues," *Appl. Opt.* **39**(16), 2853–2857 (2000).

19. C. Kim et al., "Optical phantoms for ultrasound-modulated optical tomography," *Proc. SPIE* **6870**, 68700M (2008).
20. K. Manickam, R. S. Machireddy, and S. Seshadri, "Study of ultrasound stiffness imaging methods using tissue mimicking phantoms," *Ultrasonics* **54**(2), 621–631 (2013).
21. M. D. S. H. Montes, C. P. Lopez, and F. M. Santoyo, "Finding the position of tumor inhomogeneities in a gel-like model of a human breast using 3-D pulsed digital holography," *J. Biomed. Opt.* **12**(2), 024027 (2007).
22. B. Kemper et al., "Quantitative determination of out-of-plane displacements by endoscopic-speckle-pattern-interferometry," *Opt. Commun.* **194**, 75–82 (2001).
23. C. Quan et al., "Phase extraction from a single fringe pattern based on guidance of an extreme map," *Appl. Opt.* **44**(23), 4814–4821 (2005).
24. R. Kumar and C. Shakher, "Measurement of out-of-plane dynamic deformations by digital speckle pattern interferometry," *Defence Sci. J.* **53**(1), 95–103 (2003).
25. M. J. Huang, "On the phase unwrapping of speckle interferometry maps," in *SEM X Int. Congress & Exposition on Experimental & Applied Mechanics*, https://sem.org/on-the-phase-unwrapping-of-speckle-interferometry-maps-9-pages/ (2004).
26. M. Bahich, M. Afifi, and E. Barj, "Optical phase extraction algorithm based on the continuous wavelet and the Hilbert transform," *J. Comput.* **2**(5), 1–5 (2010).
27. D. C. Ghiglia and M. D. Pritt, *Two Dimensional Phase Unwrapping: Theory, Algorithms and Software*, John Wiley and Sons, New York (1998).
28. G. Q. Gu and K. F. Wang, "Study of phase-shifting techniques in digital speckle pattern interferometry for deformation measurement, " in *Int. Conf. on Advanced Phase Measurement Methods in Optics and Imaging*, P. K. Rastogi and E. Hack, Eds., pp. 57–61, American Institute of Physics (2010).

Udayakumar Karuppanan received his BE and ME degrees in mechanical engineering from Anna University, India, in 2005 and 2010, respectively. He is currently pursuing his PhD at the Department of Applied Mechanics, Indian Institute of Technology Madras, India. His research interests are speckle interferometry for biomedical application and biomedical instrumentation. He is currently the president of the SPIE student chapter, IIT Madras.

Sujatha Narayanan Unni received her PhD from the NTU Singapore in bio-optics in 2005. She is an associate professor of biomedical engineering with the Department of Applied Mechanics, IIT Madras, India. Her research interests are in the areas of biomedical spectroscopy, bio-optical instrumentation, nondestructive optical imaging and processing of optical signals/images. She has published in reputed optics journals and conferences and several of her international conference publications have won best paper awards. She is a regular reviewer of several optics journals. She is a regular member of SPIE and OSA as well as fellow member of OSI.

Ganesan R. Angarai received his MSc and PhD degrees from the University of Madras and the Indian Institute of Technology Madras in 1984 and 1989, respectively. He is an associate professor at the Indian Institute of Technology Madras, Chennai, India. He is the author of more than 40 journal papers and the coauthor of the Indian edition of the book *Optics* with Eugene Hecht. His areas of research are laser applications in engineering metrology, holography, adaptive optics, optical instrumentation, speckle metrology, nondestructive testing, fiber optics and laser instrumentation, and biomedical instrumentation. He is a member of SPIE and also an associate editor of optical engineering.